Ab Initio Molecular Orbital Study of the Unified Mechanism and Pathways for Gas−Carbon Reactions†

Ning Chen and Ralph T. Yang*

Department of Chemical Engineering, University of Michigan, Ann Arbor, Michigan 48109-2136

Received: March 17, 1998; In Final Form: May 20, 1998

Ab Initio molecular orbital calculations are performed at the B3LYP/6-31G(d)/HF/3-21G(d) calculation level on graphite and oxygen intermediates on and near the edges of graphite. The results are in agreement with experimental data for structural geometry parameters, vibrational frequencies, and, more importantly, bond energies. Three intermediates are studied: semiquinone, carbonyl, and an off-plane, epoxy oxygen. The rate-limiting step for all gasification reactions by oxygen-containing gases is the breakage of C−C bonds to free CO from the semiquinone intermediate. The energy for this C−C bond is near 80 kcal/mol, which is close to the experimental activation energy for the reactions with CO_2 and H_2O. The C−C bond is weakened by 33% by the adjacent epoxy oxygen, to a bond energy of nearly 53 kcal/mol. This extent of weakening in the C−C bond energy coincides with the decrease in the experimental activation energy from 85 kcal/mol for the reactions with CO_2 and H_2O to 58 kcal/mol for the reaction with O_2. The equilibrium constant of dissociative chemisorption of O_2 on edge carbon is several orders of magnitude higher than that of CO_2 and H_2O. Hence the epoxy oxide intermediate only exists in the C + O_2 reaction. The C−C bond breakage that is weakened by epoxy oxygen gives rise to the low-temperature TPD (temperature programmed desorption) peak (near 450 °C), whereas the high-temperature peak (near 950 °C) is due to that without the epoxy intermediate. Two different reaction pathways are proposed for the C + O_2 and C + CO_2/H_2O reactions. All three oxygen intermediates play important roles in these pathways.

Introduction

The gasification reactions of carbon, i.e., the reactions of carbon with O_2, H_2O, CO_2, and H_2, have been studied extensively because of their importance in energy generation, metallurgy, and catalysis. A multitude of experimental techniques have been employed, and much is already understood on the kinetics and mechanism of these reactions.[1−10] Among the experimental techniques used were temperature programmed desorption (TPD), thermogravimetric analysis (TGA), transient kinetics (TK), and microscopic techniques such as transmission electron microscopy (TEM)[2] and scanning tunneling microscopy (STM).[11,12] Theoretical studies, in contrast, have been very limited. Molecular orbital calculations[13] on graphite based on quantum mechanics started to appear some 20 years ago.[14] More recently, a series of molecular orbital studies have been performed on gas−carbon reactions with the aim of gaining a basic understanding of the reaction intermediates and hence the reaction mechanism.[15−18] However, semiempirical molecular orbital theories were used in these studies.

There are several important experimental facts that remain poorly explained regarding the carbon gasification reactions. The kinetic behaviors of the C + CO_2 and C + H_2O reactions are similar and are very different from that of the C + O_2 reactions in many ways.[1] The activation energy for the C−O_2 reaction is 50−58 kcal/mol, and that for the C−CO_2 and C−H_2O reactions is in the range of 80−86 kcal/mol. The C−O_2 reaction is also orders of magnitude faster than the two other reactions. It should be pointed out that the absolute values of activation energies for these three reactions may vary from sample to sample, but the relative values always follow the same order; i.e., C−O_2 reaction has a lower activation energy than the C−CO_2 and C−H_2O reactions. Moreover, TPD results show a CO desorption peak near 950 °C for all three gas−carbon reactions and a broad shoulder at the lower temperature near 450 °C for the C−O_2 reaction only. Obviously, two or more oxygen-containing intermediates exist for these carbon gasifications. Semiquinone and carbonyl types of intermediates have been observed, and an off-plane type intermediate was more recently proposed in our laboratory.[17,18,20] On the basis of this off-plane oxygen species, a unified mechanism[17,18] was proposed that was able to account qualitatively for all key experimental facts on the kinetic behaviors of the reactions. Unfortunately, since the semiempirical molecular orbital theories are not accurate in energy calculations, the C−C bond energies in our previous studies were of the order of 550 kcal/mol, which was about four times higher than the experimental value.[17,18] Furthermore, the proposed mechanism did not take into account the existence of the carbonyl intermediate and the difference between the semiquinone and carbonyl types of intermediate. Another interesting yet poorly understood experimental observation pertains to the shape of the etch pits on the basal plane of graphite that are created by different gases. The two hydrogen-containing gases (H_2O and H_2) form hexagonal shaped pits, whereas circular pits are formed by the other gases (CO_2, H_2O, and NO).

* To whom all correspondence should be addressed.

† Abbreviations: TPD = temperature-programmed desorption; TGA = thermogravity analysis; TK = transient kinetics; TEM = transmission electronic microscopy; AIM = atom in molecule method; STM = scanning tunneling microscopy; SCF = self-consistent-field; σ_n = standard deviation; IR = infrared; Gaussian 94 = ab initio molecular orbital calculation software; CNDO = complete neglect of differential overlap; EHMO = extended Hückel Molecular Orbital method; MOPAC = semiempirical molecular orbital calculation software.

S1089-5639(98)01518-7 CCC: $15.00
Published on Web 07/15/1998

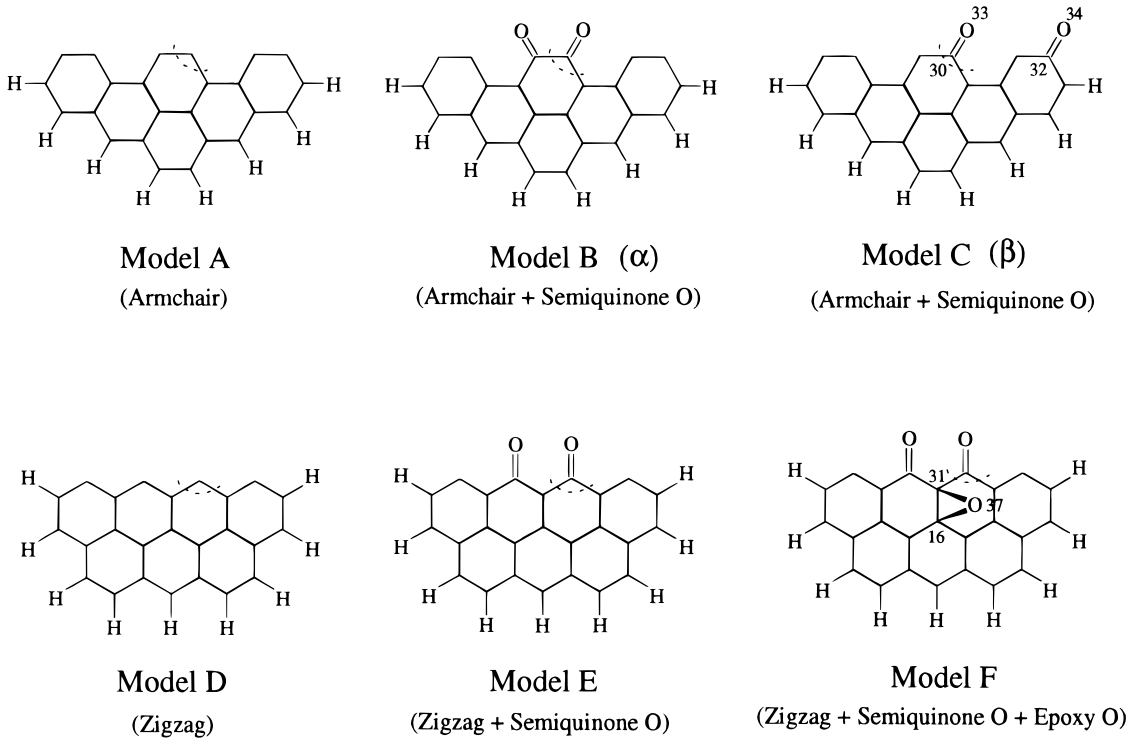

Figure 1. Selected graphite models for calculation, including three oxygen intermediates. The dotted line indicates where the C−C bond breakage takes place to free CO. Epoxy O_{37} is perpendicular to the basal plane. Semiquinone and carbonyl oxygen are bonded to carbon with a double bond.

Ab initio molecular orbital theories are capable of substantially more accurate energy calculations than the semiempirical theories.[13] In the present study, we used the ab initio theory to calculate all oxygen-containing and hydrogen-containing intermediates, and all the important experimental observations are satisfactorily explained by these results. Moreover, the unified mechanism that we have proposed previously based on semiempirical molecular orbital calculations is fully supported by the ab initio theory.

Model Chemistry, Molecular System, and Calculation Levels

The molecular orbital calculations based on quantum mechanics were developed originally for isolated molecular systems. Therefore, for molecular systems containing solids, it is a crucial step to extract correctly a finite model piece to represent the infinite solid and to saturate correctly the boundaries for the model. In addition, the theoretical level of the calculation is another factor that can greatly influence the final result. The selection of a proper "model chemistry" and "molecular system" for graphite has been carefully studied in our previous work[21] with various graphite models of different types and sizes and at various calculation levels. Accordingly, the model $C_{25}H_9$ (see Figure 1) became our selected molecular system because it yielded the closest results to the experimental data, and the calculation level B3LYP/6-31G(d)//HF/3-21G(d) yielded the best overall performance on both final results and computational cost. Furthermore, hydrogen termination was used successfully to saturate the boundaries of the graphite model. Therefore, starting from the model $C_{25}H_9$ with the B3LYP/6-31G(d)//HF/3-21G(d) calculation level, various graphite models, including zigzag edge, armchair edge, semiquinone (in-plane) oxygen intermediate, and epoxy (off-plane) oxygen intermediate, shown in Figure 1, are studied in this work. The reasons for choosing these models are well-documented in our previous work[21] and will also be supported in this work. Hydrogen termination is also used in this study. All calculations include the following steps: checking the stability of wave functions, geometric optimization for optimizing the molecular system to a minimal on the potential energy surface, frequency calculation for the vibrational spectra properties and thermochemical properties, and "higher level" single point calculations with B3LYP/6-31G(d) model chemistry for more accurate total energies according to well-established conventional procedures.

Bond Energy Calculations

Even with the most advanced AIM (atoms in molecule) method, which can deal with some localized properties within the studied molecule, the bond energy property, a classic chemistry property, is still not available in most molecular orbital calculation packages, such as the Gaussian 94 package. The bond energy (as a direct measurement of the bond strength) is very useful in correlating the chemical reaction with molecular and atomic level properties. In our previous work[17,18] we adopted the methodology of breaking the molecular system into separate pieces at the C−C bond and calculating the C−C bond "dissociation" energy accordingly. When the molecule was broken down into several pieces, however, the chemical environmental also changed, and this might introduce errors in the subsequent energy deduction. Therefore, in this study, we designed a better procedure, described as follows.

For the carbon gasification reactions, the C−C bonds on the surface need to be broken in order to liberate the CO molecule from the surface. Two edge sites comprise the active sites on the surface of graphite, shown in Figure 1, i.e., the armchair and zigzag edges. The following procedure is used to calculate the C−C bond energies for a CO molecule to break off from the edges.

(1) For a geometrically optimized molecular system, we equilaterally change (either increase or decrease) the bond lengths of the two C−C bonds that hold the C═O molecule on the edges (Figure 1).

TABLE 1: Calculated Geometric Parameters for Graphite Models and Oxygen Intermediates (Figure 1) at the HF/3-21G(d) Level[a]

			armchair			zigzag			
	bond		$C_{24}H_8$, model A	IP Oα $C_{24}H_8O_2\alpha$, model B	IP Oβ $C_{24}H_80_2\beta$, model C	$C_{25}H_9$, model D	IP O $C_{25}H_9O_2$, model E	IP + OP O $C_{25}H_9O_3$, model F	exptl data[23]
BL (Å)	C−C	av	1.402	1.416	1.413	1.416	1.414	1.424	1.42
		SigmaN	0.0329	0.0392	0.0321	0.0184	0.0206	0.0348	
		DTED (%)	1.3	0.3	0.5	0.3	0.4	0.3	
	C−H	av	1.072	1.072	1.072	1.073	1.072	1.072	1.07
		SigmaN	0.0007	0.0006	0.0015	0.0007	0.0009	0.001	
		DTED (%)	0.2	0.2	0.2	0.2	0.2	0.2	
	C−O(IP)	av		1.2302	1.292 (C30−O33) 1.298 (C32−O34)		1.2759	1.246	1.13 (CO)
	C−O(OP)	av						1.509 (C16−O37) 1.491 (C31−O37)	1.43 ($(CH_3)_2O$)
BA(o)	C−C−C	av	120.38	120.14	120.46	120.53	120.22	120.1	120
		SigmaN	1.4903	1.8818	2.7265	2.3263	2.2751	1.8549	
		DTED (%)	0.3	0.1	0.4	0.4	0.2	0.1	
	C−C−H	av	119.42	119.57	119.52	119.52	119.51	119.66	120
		SigmaN	1.2764	1.1371	1.1421	0.6752	0.7195	0.8344	
		DTED (%)	0.5	0.4	0.4	0.4	0.4	0.3	
	C−C−O (IP)	av		121.81	121.71		121.35	121.29	120 (CO)
	C−C−O (OP)	av						59.35 (C31−C16−O37) 60.56 (C16−C31−O37)	110 ($(CH_3)_2O$)
DA	property	plane	plane	plane	plane	plane	plane	nonplane	

[a] Note: BL, bond length; BA, bond angle; DA, dihedral angle; IP, in-plane oxygen; OP, off-plane oxygen; av, average; SigmaN, standard deviation; DTED, deviation to experimental data; plane, 0 or 180° dihedral angle.

(2) Upon each bond length change, we perform the single point total SCF energy calculation for the whole molecular system. It can be expected that the system energy will increase when the C−C bond length changes (in any direction) since the molecule moves away from its geometrically optimized position, which represents the minimal on the potential surface.

(3) Step 2 is performed until there is no further change in the total energy upon C−C bond length changes. Hence, the total energy reaches the level when the two C−CO bonds are thoroughly dissociated from the molecular system. The C−C bond energy is subsequently obtained from the energy curves vs the bond lengths.

(4) Finally, since this method cannot be distinguished between the two adjacent bonds of C−CO, we simply divide this total energy by 2 to assign the energy as the "bond energy" of the C−CO bond in the graphite models. By doing this, a more accurate bond energy is obtained. The shortcoming of this method is the high cost of computational resources, since over 40 single point calculations will be needed for each bond energy calculation and each individual single point SCF energy calculation with B3LYP/6-31G(d) will take about 24 h of CPU time on our workstation.

"Gaussian 94" molecular orbital calculation package,[22] supplied by Gaussian, Inc., was used, and all calculations were performed on a single Hewlett-Packard C160 workstation. The detailed calculation procedure was described elsewhere.[21]

Results and Discussion

First, stable wave functions are achieved for all graphite models shown in Figure 1, indicating there is a certain minimum on the potential surface that corresponds to the expected structure for each of our models. Therefore, this will guarantee the validity of our further calculations on these models.

Geometry. Full geometry optimization, i.e., optimization over all atoms, is employed. All optimizations end at a minimum on the potential surface, indicating the stability of our selected graphite models. The analysis of geometric parameters for each individual bond is not meaningful, because our graphite model is finite, and the geometric parameters are not uniform for different bonds in the model. Therefore, the statistical analyses of the geometric parameters are listed in Table 1.

There are several points that need discussion. First, the calculated geometric parameters among all different models are in agreement; this implies that our models are well-selected and are representative. Second, the deviations from experimental data for bonds that involve hydrogen are minimal, i.e., 0.2−0.4%. This indicates that the use of hydrogen atoms as terminators for the graphite model boundaries will not significantly affect our overall calculation results. Next, calculated bond length (C−C, C−H, and C−O) and bond angle (C−C−C, C−C−H, and in-plane C−C−O) are in agreement with the experimental data[23] and are also consistent among the different models. For example, the C−C bond lengths are around 1.42 Å with less than 1.3% maximum deviation from experimental data and less than 0.04 standard deviation; the C−C−C bond angles are around 120° with less than 1% maximum deviation from experimental data. Here a dihedral angle is the angle between two planes, each of which is formed by connecting three atoms. Fourth, the in-plane C−O bond lengths (1.2^+ Å) are longer than that of free CO (carbon monoxide, 1.13 Å), implying the intermediate property of the in-plane oxygen toward full dissociation of CO. Likewise, the bond length (1.49^+ Å) of epoxy oxygen (i.e., the off-plane oxygen) is also longer than that for epoxide (1.43 Å), evidence of an intermediate property of epoxy oxygen species. Finally, the dihedral angles for all models, except the epoxy oxygen-containing model (model F), are either 0 or 180°, indicating the single plane sheet character of graphite. With the epoxy oxygen (i.e., off-plane oxygen; see model F in Figure 1), the basal plane is not perfectly flat, with the two carbon atoms bonded to epoxide bulging from the basal plane of graphite by a distance of up to 0.24 Å in the c-direction. This is the result of interaction between the graphite substrate and the epoxy oxygen. There are several pieces of experimental evidence of the nonperfect-plane property of graphite with up to 0.3 Å of height difference in the *c*-direction

TABLE 2: Infrared and Raman Vibrational Frequency Calculations for C−C and C−O Bonds in Graphite Models (Figure 1)[a]

	armchair			zigzag		
	$C_{24}H_8$, model A	IP O α $C_{24}H_8O_2α$, model B	$C_{25}H_9$, model D	IP O $C_{25}H_9O_2$, model E	IP + OP O $C_{25}H_9O_3$, model F	exptl data
			Frequency/Raman Activity[b]			
	1233/60					
	1252/23	1141/5		1306/85	1427/8	
	1345/23	1237/7		1347/22	1444/16	
A_1 g mode	1353/51	1257/12	1399/22	1399/100	1451/18	1360
				1405/60		
	1473/21		1440/42			
	1595/48	1420/7	1451/23		1469/13	
E_2 g mode	1659/100	1643/100	1465/100	1501/6	1479/100	1580
			1467/31		1493/69	
			1482/29			
			Frequency/Infrared Intensity[b]			
		1318/7		1346/45		
		1425/7		1393/17	1319/33	
C−O asymmetric stretching		1433/8		1452/43	1364/53	1445
		1507/15		1631/21		
C−O symmetric stretching		1642/100		1563/100	1493/25	1535
epoxide					1271/100	1250

[a] Note: IP, in-plane; OP, off-plane. [b] The Raman activity and IR intensity are scaled to the strongest band (as 100%). Frequencies are in cm^{-1}.

TABLE 3: C−C Bonds per C Atom. Effect of the Size of the Graphite Model on Bond Energy Calculation

model size (rings)	1	3	6	10	15	21	28	70	infinity
C atoms	6	13	22	33	46	61	78	193	infinity
C−C bonds	6	15	27	42	60	81	105	270	infinity
ratio (bond/atom)	1	1.1538	1.2273	1.2727	1.3043	1.3279	1.3462	1.399	1.5

(basal plane) as observed under the STM (scanning tunneling microscopy).[24,25] This phenomenon, referred to as corrugation, was the result of either atomic or electric configurations from the electric field of STM.

Vibrational Frequency Calculations. The scale factor of 0.9085 is appropriate for calibrating the systematic errors for the HF/3-21G(d) level model chemistry[26] and is hence used in this study. Since graphite is infrared (IR) nontransparent, there is very little IR experimental data in the literature for graphite. However, two distinguishing Raman active vibrational frequencies from experiment[27,28] at 1360 (A_1 g mode) and 1580 cm^{-1} (E_2 g mode) can be compared with our calculated results. On the other hand, for oxygen-containing models (models B, E, and F in Figure 1), infrared experimental data are available. There are two adsorption bands at 1445 and 1535 cm^{-1} for asymmetric and symmetric CO stretching frequencies, respectively,[29] and one very strong band at 1250 cm^{-1} for the asymmetric C−O−C stretching frequency for epoxide;[30] the latter corresponds to our epoxy oxygen intermediate. As in our previous work,[21] the vibrational frequencies related to the boundary saturation group C−H, i.e., the C−H stretching frequencies above 3200 cm^{-1} and the C−H out-plane deformation frequencies below 1000 cm^{-1}, will not be discussed. The assignment of frequency is mainly based on the analysis of vibrational normal mode, symmetry, intensity (infrared), or activity (Raman) and the discrimination between any frequencies separated by less than about 200 cm^{-1} wavenumbers. The detailed frequency analysis results (infrared and Raman), including frequency, relative intensity/activity, and vibrational mode assignment, are summarized in Table 2. (The detailed data are available upon request.)

For all five models (models A−F), there are two distinguishing Raman bands for the A_1 g and E_2 g modes of graphite. The deviations of the 1360 cm^{-1} A_1 g and 1580 cm^{-1} E_2 g modes are less than a 120 cm^{-1} shift. These deviations are not significant since generally a tolerance of 200 cm^{-1} is allowed for frequency calculations and also considering the relatively low calculation level (HF/3-21 G(d)) that is being used. Two interesting results emerge:[1] The IR C−O stretching (symmetric and asymmetric) mode frequencies for the in-plane C−C−O (models B, E, and F) are surprisingly close to the experimental data for free carbon monoxide. This result suggests that the in-plane C−O bond already possesses some carbon monoxide character.[2] The appearance of the 1271 cm^{-1} band for the epoxy oxygen containing model (model F) is in agreement with the infrared experimental data of 1250 cm^{-1} characteristic frequency for epoxide. Other C−O stretches are also possible for this frequency, such as that in anhydrides and ethers, but are unlikely as intermediates for the gas−carbon reactions. Therefore, it is reasonable to conclude that off-plane oxygen is actually interacting with the basal plane carbon to form an epoxide type chemical structure, which is the reason why we propose the more meaningful term "epoxy" oxygen intermediate for the "off-plane oxygen" intermediate.

Bond Energy Calculations. The bond energy of graphite is a much studied classic topic. For example, literature reports include the heat of dissociation of graphite to carbon atoms as 170.4 kcal/mol at 0 K,[31] the heat of sublimation of graphite to a monatomic gas being 171.7 kcal/mol at 300 K,[32] and even the heat of combustion (with oxygen) of graphite being 94.1 kcal/mol at 25 °C.[33] Therefore, it is reasonable to take 170 kcal/mol as the reference bond energy for the C−C bond in graphite. However, when comparing our calculated bond energy data to this experimental value, there is one factor that needs to be taken into account: the calculated bond energy is actually in the units of kilocalories "per bond" instead of "per mole" or "per atom". The ratio of the number of carbon atoms and the number of C−C bonds actually changes with the size and shape of the graphite model. Table 3 clearly shows this fact. From Table 3, the limiting correlation ratio of bond/atom is 1.5. Hence suitable correlation ratios of bond/atom should be

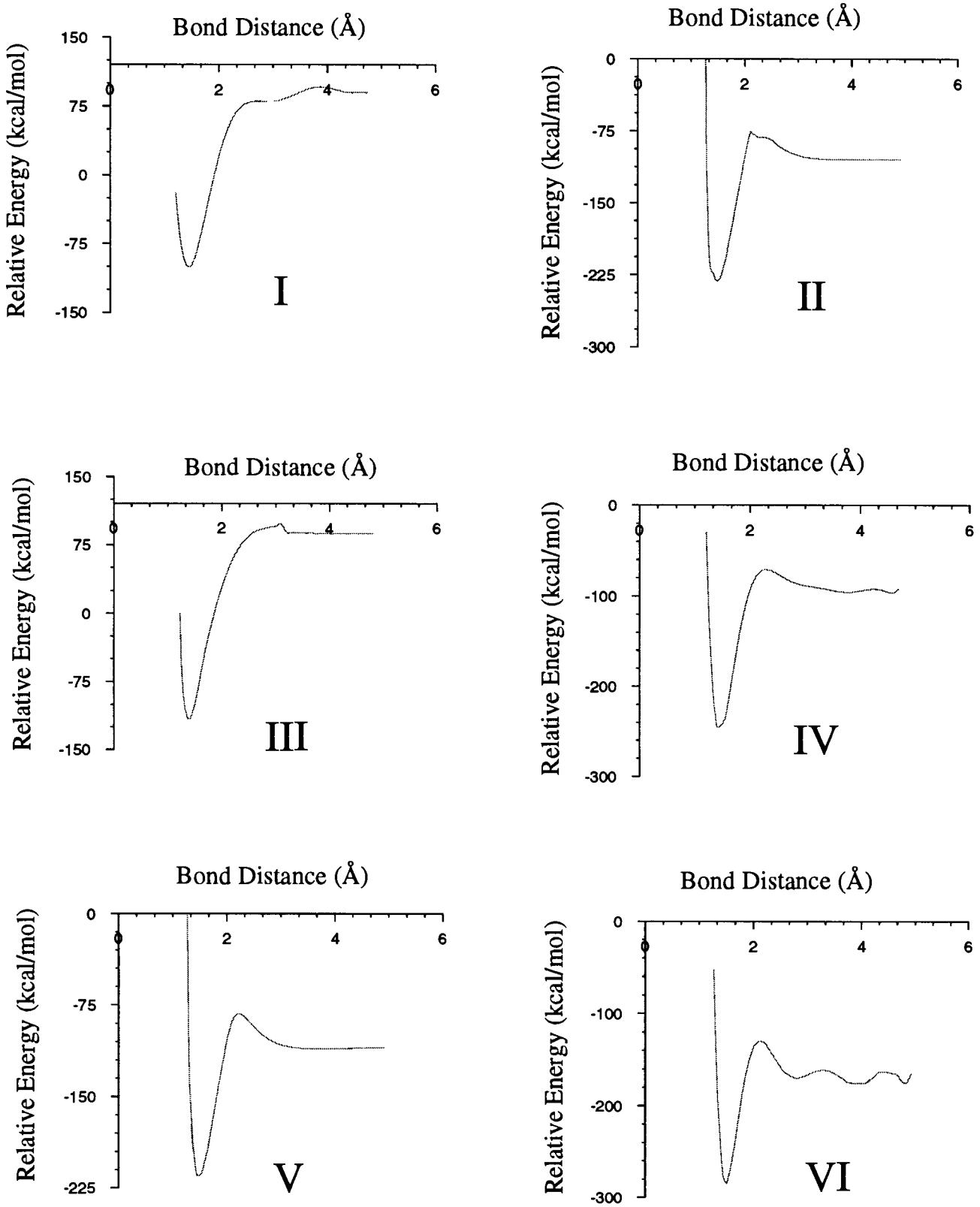

Figure 2. Energy curves vs C−C bond distance (along dotted lines in Figure 1) for different models (see Figure 1) and at different calculation levels: (I) model A at B3LYP/6-31G(d); (II) model C at B3LYP/6-31G(d); (III) model D at B3LYP/6-31G(d); (IV) model E at B3LYP/6-31G(d); (V) model F at B3LYP6-31G(d); (VI) model F at HF/3-21G*.

multiplied to the calculated bond energy data for different graphite models.

Figure 2 shows the energy curves (vs C−C bond length) for different models and at different calculation levels. As the C−C bond length is changed, the system energy decreases to form a deep and narrow potential well. This is similar to the typical potential curve for interactions between two atoms. When the bond length is further increased, this energy curve approaches a certain energy level which is the energy for the totally dissociated model. Therefore, it is reasonable to take the difference between the lowest energy point and the dissociated end energy on the energy curve for the C−C bond energy

TABLE 4: Calculated C−C Bond Energies for Gasification (Indicated by Dotted Lines in Figure 1) for Different Models

		armchair			zigzag			
		$C_{24}H_8$, model A	IP Oα $C_{24}H_8O_2$, model B	IP Oβ $C_{24}H_8O_2\beta$, model C	$C_{25}H_9$, model D	IP O $C_{25}H_9O_2$, model E	IP + OP O $C_{25}H_9O_3$, model F	weakening of C−CO by epoxy O
HF/3-21G(d)	raw data	97.4	39.3	63.1	132.1	80.8	53.8	33.40%
	calibrated[a]	118.9			163.8			
B3LYP/6-31G(d)	raw data	96.5		63.4	101.9	77.87	52.2	32.90%
	calibrated[a]	116.8			126.4			

[a] Calibration factors are as follows: 1.21 for C_{24} and 1.24 for $C_{25}H_9$ (see Figure 1). The experimental C−C bond energy is approximately 170 kcal/mol. IP, in-plane oxygen; OP, off-plane oxygen.

calculation. (The dissociated end energy is actually averaged over values at bond distances greater than 0.3 nm.) Moreover, the higher calculation level (B3LYP/6-31G(d)) yields a smoother curve than does the lower level (HF/3-21G(d)), as seen by comparing the curves V an VI. It is obvious that the higher calculation level would result in a more accurate bond energy. The computational cost, however, is approximately 20 times higher for the higher calculation level (B3LYP/6-31G(d) vs HF/3-21G(d)). It is noted that even the lower calculation level can yield quite good energy results, as seen in Table 4, which summarizes the C−C bond energy calculations.

From Table 4, the bond energies for the two pure graphite models (A and D) are of the orders of 120 and 130 kcal/mol, respectively, using the B3LYP/6-31G(d) calculation level.

The C−C bond energies calculated by using semiempirical molecular orbital methods such as CNDO[17] and MOPAC[18] are of the order of 550 kcal/mol. The values from the ab initio calculations (i.e., 120−130 kcal/mol) are clearly much closer to the experimental value, which is approximately 170 kcal/mol. Considering the model size effect (Table 3), it appears that, for bond energy calculations, a still larger size is desirable (due to a higher correlation ratio).

The C−C bond energies are calculated by breaking the bonds on the edges of graphite indicated by the dotted lines in Figure 1. It is clearly seen that the edge C−C bonds are substantially weakened when one of these edge carbon's is bonded to an oxygen atom. The energy for this C−C bond is ∼80 kcal/mol, which is close to the activation energies for the reactions with CO_2 and H_2O. More importantly, the edge C−C bond is further weakened significantly by the off-plane, epoxy oxygen (model F, Figure 1). From the results in Table 4, the C−C bond is weakened by approximately 33% by the epoxy oxide, to a bond energy of nearly 53 kcal/mol. The extent of weakening in the C−C bond energy coincides with the activation energy decrease from 85 kcal/mol for the reactions with CO_2 and H_2O to 58 kcal/mol for the reaction with O_2. The extent of C−C bond weakening is higher than that predicted by semiempirical molecular orbital calculations that we performed previously,[18] which is about 20%.

It should be noted that the saturated semiquinone on the armchair edge yields the weakest C−C bonds. The bond energy for model B is only 39.3 kcal/mol (Table 4). To saturate all armchair edge atoms by semiquinone type oxygen is obviously unfeasible for steric reasons. The fact that the $C-O_2$ reaction and the $C-CO_2$ reaction both yield circular etch pits indicates that this type of intermediate is not formed (since otherwise the pits would have been hexagonal in shaped bound by zigzag edges). Furthermore, an in-plane type epoxy oxygen bonded to two unsaturated edge carbon atoms on the armchair edge is certainly another possible intermediate. This is not included in the present calculation.

Comparing the C−C bond energies of model C and model E (Table 4), it is seen that the bond energies are similar, i.e., 63.4 kcal/mol vs 77.8 kcal/mol at the B3LYP/6-31G(d) calculation level. This result indicates that the gasification of carbon on both armchair and zigzag edges are of equal ease. Consequently, the etch pits for the $C + O_2$ and $C + CO_2$ reactions are circular in shape.

The reason for the etch pits formed by the $C + H_2O$ reaction being hexagonal in shape and being bound by zigzag edges is due to chemisorbed H atoms on the edge C atoms.[15,16] The C−H bond on the zigzag edge is substantially more stable; hence the armchair edges are preferentially gasified.[15,16]

Unified Mechanism. In our earlier work,[18] a unified carbon gasification by oxygen-containing gases was proposed. Two types of oxygen intermediates are involved: in-plane oxygen (either semiquinone or carbonyl) and off-plane oxygen (i.e., epoxy oxygen), as shown in Figure 1E,F. The rate-limiting step is the breaking of the C−C bonds on the edges to release the CO molecule. This is the case with $C + CO_2$ and $C + H_2O$ reactions with an activation energy of 85 kcal/mol. For the $C + O_2$ reaction, due to the high dissociative chemisorption constant of O_2 on carbon,[1] there is an abundance of the epoxy oxygen; hence the C−C bonds are significantly weakened, which results in a lower activation energy (58 kcal/mol). However, several shortcomings of the earlier work are obvious. First, the semiempirical molecular orbital calculations that were used, MOPAC of PM3 and CNDO,[34] were not accurate due to drastic assumptions and approximations. Some of the results generated by those methods are far from the experimental data; for example, the C−CO bond energy of 550 kcal/mol is much higher (by almost 4 times) than the realistic value of 100 kcal/mol. Second, the proposed mechanism accounted for only "in-plane" and "off-plane" oxygen intermediates; no explanation for the difference between and the roles of the semiquinone and carbonyl oxygen intermediates in the gasification reactions was offered. But those two oxygen intermediates (both are in-plane types) are important for carbon gasification reactions as they have been identified experimentally.

The ab initio molecular orbital calculation results shown in the foregoing have provided much more accurate results. These results also provide a further understanding for the mechanism with new proposed reaction pathways, which take into account semiquinone (in-plane), carbonyl (in-plane), and epoxy (off plane) oxygen intermediates. First, the C−CO bond energies are on the order of 100 kcal/mol; see Table 4. Second, the presence of the epoxy oxygen indeed significantly weakens the C−CO bond energy. The extent of weakening is 33% for both calculation levels rather than 20% by our previous result, as indicated in the last column in Table 4. It is significant that this degree of weakening is the same as the 32% decrease in activation energies, i.e., from 85 kcal/mol for the $C + CO_2$ and $C + H_2O$ reactions to 58 kcal/mol for the $C + O_2$ reaction. This result also suggests that the C−CO bond breakage is the rate-determining step. Third, in our previous work, the off-

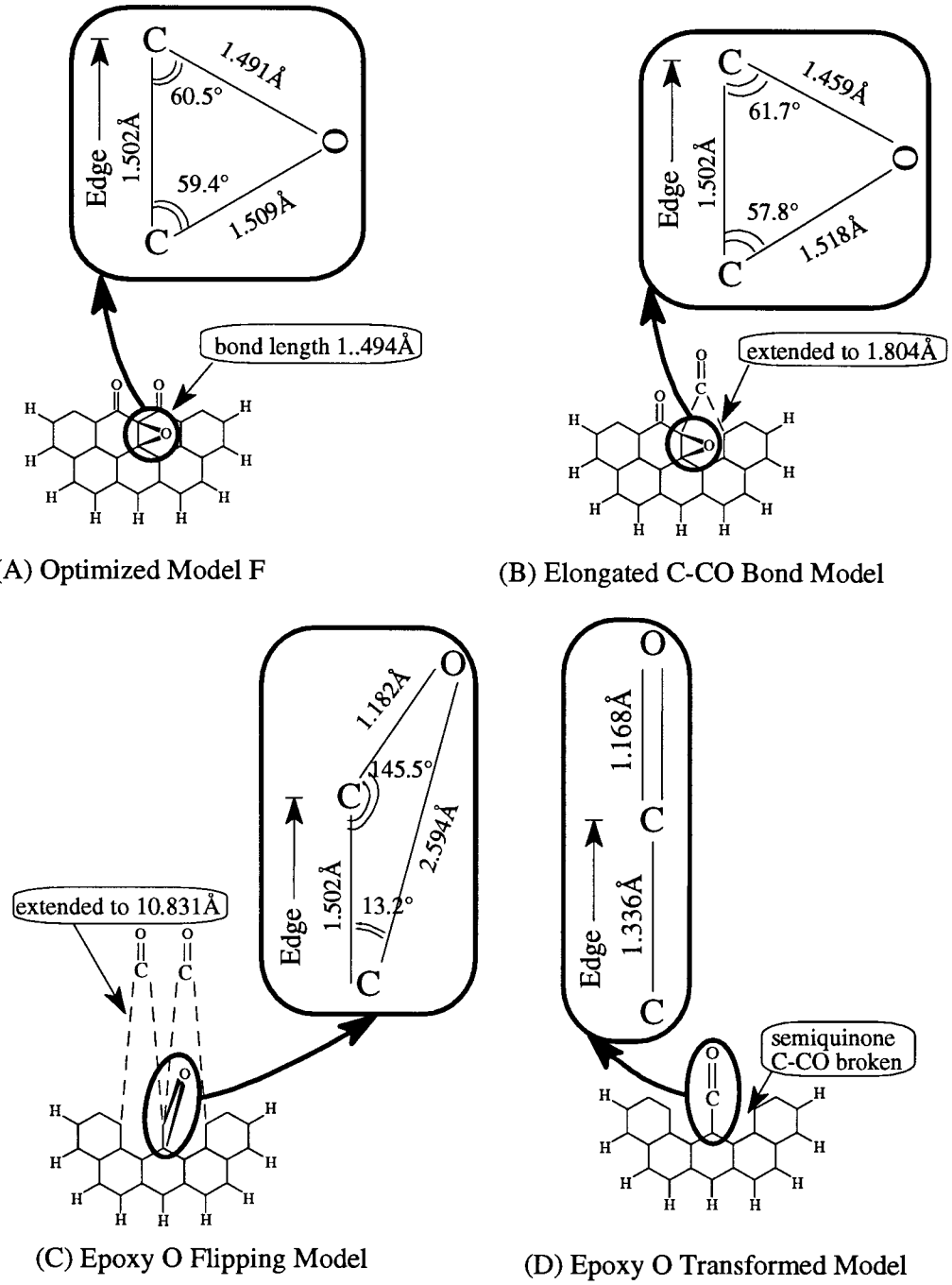

Figure 3. Steps showing the transformation of the off-plane epoxy oxygen into in-plane carbonyl oxygen, by freeing the semiquinone CO.

plane (epoxy) oxygen was optimized with equal distance to two basal plane carbon atoms. The present calculation indicates that the epoxy oxygen actually tilts toward the edge site slightly, as shown in Table 1 (column 9) and Figure 3A.

The reaction pathway for the case with the epoxy oxygen intermediate is illustrated in Figure 3. Ab initio calculations are performed to see how the weakened C−C bonds break (to release the semiquinone CO). As the two C−C bonds are elongated (Figure 3B,C), the epoxy oxygen tilts further toward the outer edge of the basal plane. As the elongation continues, the epoxy oxygen nearly flips over to the basal plane (Figure 3C). At this position, the epoxy oxide has already gained a strong characteristic of the C═O double bond with a 1.18 Å bond length. Finally, it is expected that this epoxy oxygen transforms into an in-plane oxygen, i.e., carbonyl, as the two C−C bonds break to release CO, as shown by Figure 3D.

Oxygen intermediates are formed by dissociative chemisorption of oxygen-containing molecules:

$$C + O_2 \leftrightarrow C(O)$$

$$C + CO_2 \leftrightarrow C(O) + CO$$

$$C + H_2O \leftrightarrow C(O) + H_2$$

The equilibrium constants for dissociative chemisorption are very different for O_2 and CO_2/H_2O. Such values for O_2 are orders of magnitude higher than that for CO_2 and H_2O.[1] (The ratio of the equilibrium constants for H_2O over CO_2 is approximately 3, which is the equilibrium constant for water−gas shift reaction. Because of the high equilibrium constants for the $C-O_2$ system, the concentrations of the oxygen

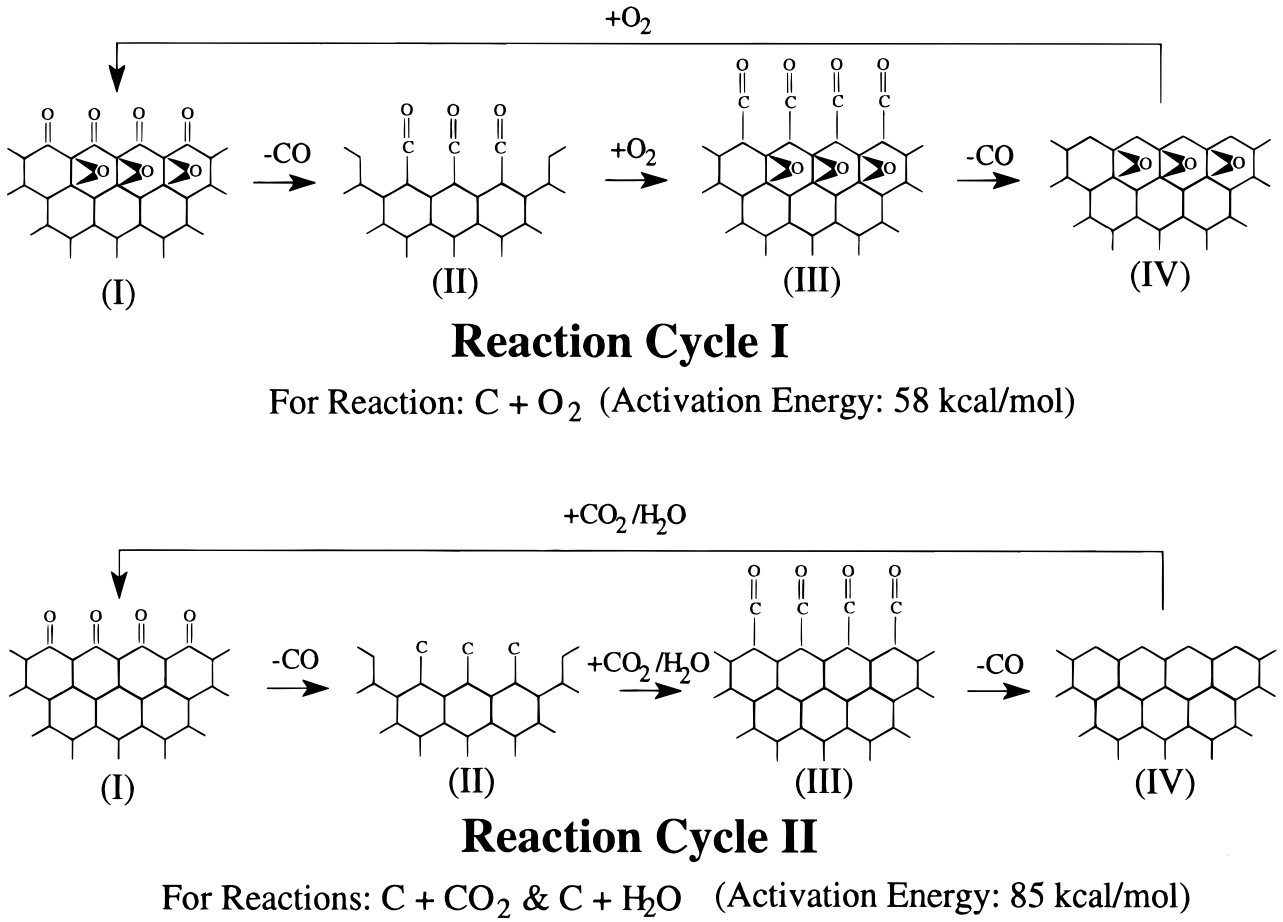

Figure 4. Complete reaction pathways for graphite gasification, indicating three oxygen intermediates.

complexes are also high. The high concentration of the dissociated surface oxygen atoms form the epoxy oxygen intermediates. Therefore it is reasonable to expect that the concentration of the epoxy oxygen intermediate is much higher in the C + O_2 reaction than in the C + CO_2 and C + H_2O reactions. In fact, experimental results on TPD and reaction activation energies, to be discussed shortly, indicate that the epoxy oxygen only exists in the C + O_2 reaction.

Reaction Pathways. Two reaction pathways are deduced from the calculation results, one for the C + O_2 reaction and one for the C + CO_2 and C + H_2O reactions. These two pathways are shown in Figure 4. The zigzag edge is used as an example, while the same pathways also apply to the armchair edge.

For the C + O reaction (Figure 4A), the in-plane semiquinone oxygen (I) dissociates first with a low activation energy of 58 kcal/mol because of the C−CO bond weakening by the epoxy oxygen; at the same time the epoxy oxygen flips over to the edge to transform into in-plane carbonyl oxygen (II). Next, further chemisorption of oxygen will generate new epoxy oxygen (III), while the carbonyl breaks off to regenerate the active edge carbon sites (IV). Dissociative chemisorption of O_2 immediately follows to form the semiquinone oxygen (I). The C−C bond in C−C═O (structure II) is weaker than either one of the two C−C bonds in structure I. However, the breakage of carbonyl bond (II and III in Figure 4) only involves one C−C bond to release CO, while the breakage to free the semiquinone oxygen requires breaking two C−C bonds to free one CO. Hence this is the rate-limiting step.

For the C + CO_2 and C + H_2O reactions, there is no significant amount of the epoxy oxygen intermediate. Therefore the semiquinone oxygen (I) dissociates with an activation energy of 85 kcal/mol. A dangling carbon bond is formed which leads to carbonyl by the chemisorption of oxygen. The carbonyl groups dissociate from the edges to regenerate the bare edge sites, which lead to semiquinone oxygen by dissociative chemisorption of CO_2 or H_2O. For the same reason discussed above (for the C + O_2 reaction), the rate-limiting step is the breakage of two C−C bonds to free the semiquinone CO, hence the high activation energy (85 kcal/mol).

The reaction pathways proposed here (Figure 4) can account for all key experimental results for carbon gasification reactions. First, the three oxygen intermediates are all accounted for in these pathways; each plays a role in the pathway without which the reaction cycle cannot be completed. The different activation energies are also consistent with (in fact, predicted by) the ab initio molecular orbital results. The TPD results are described below.

A large body of information is available in the literature concerning TPD of different carbons preoxidized in different gases (i.e., O_2, CO_2, and H_2O) under different conditions.[10,19,20,35−45] Although the CO desorption patterns differ in shapes and peak positions, all spectra showed a distinct peak in the neighborhood of 950 °C. This was true despite the different oxidizing gases and types of carbon samples that were used, and the carbon samples were oxidized to different burnoff levels. The total amounts of CO released as well as the widths of the desorption peak were also different. An example of the TPD studies was that by Marchon et al.,[39] who used TPD and XPS to investigate a polycrystalline graphite treated with O_2, CO_2, or H_2O. All of their TPD spectra exhibited a CO desorption peak in the range of 973−1253 K. With the aid of

XPS results, this TPD peak was assigned to the desorption of a semiquinone structure on the edge surface of graphite.

A major difference has also been observed among the TPD spectra from carbon oxidized by O_2 and those oxidized by CO_2 or H_2O. The desorption of CO from the O_2-oxidized samples starts substantially at lower temperatures, as low as 400 °C, resulting in broad TPD peaks or as a shoulder on the low-temperature side of the 950 °C peak.[37−41] This result is consistent with the fact that significant carbon gasification for the $C-O_2$ system can take place at temperatures as low as 400 °C, whereas the $C-CO_2$ and $C-H_2O$ reactions occur near 700 °C and above.[1] It is also consistent with the fact that the activation energy for the $C-O_2$ reaction is generally lower than that for the $C-CO_2$ and $C-H_2O$ reactions, e.g., 58 kcal/mol vs 85 kcal/mol.[1]

The ab initio molecular orbital results show that the epoxy oxygen plays a key role in weakening the C−C bonds that are bonded to the semiquinone oxygen. The weakened bonds correspond to the low-temperature TPD peak (near 450 °C), whereas the bonds without epoxy oxygen give rise to the high-temperature TPD peak (near 950 °C). As mentioned, the breakage of the C−C bonds to free CO from the semiquinone is the rate-limiting step for all three reactions. The proposed unified mechanism and the reaction pathways can account for all important experimental facts.

The activation energy may change slightly with the reactant partial pressure, especially for $C + O_2$ reaction.[19] This is true if we relate the activation energy with the weakening of the C−CO bond by the epoxy oxygen, since the epoxy oxygen concentration is obviously dependent on the pressure. Finally, there has been evidence for the basal plane chemisorbed oxygen enhancing the gasification reactions by diffusion or migration.[18,46,47] In our reaction cycle, the transformation of the epoxy oxygen (off-plane) into the carbonyl oxygen (in-plane) may be a part of the enhancing effect, and it may also be the terminal for oxygen diffusion on the basal plane.

Acknowledgment. This work was supported by NSF Grant CTS-9523801.

References and Notes

(1) Walker, P. L., Jr.; Rusinko, F., Jr.; Austin, L. G. *Advances in Catalysis*; Academic Press: New York, 1959; Vol. 11, p 133.
(2) Yang, R. T. *Chemistry and Physics of Carbon*; Dekker: New York, 1984; Vol. 19, p 163.
(3) Laine, N. R.; Vastola, F. J.; Walker, P. L., Jr. *J. Phys. Chem.* **1963**, *67*, 2030.
(4) Radovic, L. R.; Jiang, H.; Lizzio, A. A. *Energy Fuels* **1991**, *5*, 68.
(5) Huttinger, K. L.; Nill, J. S. *Carbon* **1990**, *28*, 457.
(6) Chen, S. G.; Yang, R. T. *J. Catal.* **1990**, *141*, 102.
(7) Ergun, S.; Mentser, M. R. *Chemistry and Physics of Carbon*; Dekker: New York, 1965; Vol. 1, p 203.
(8) Walker, P. L., Jr.; Shelef, M.; Anderson, R. A. *Chem. Phys. Carbon* **1968**, *4*, 287.
(9) Baker, R. T. K. *Carbon and Coal Gasification Science and Technology*; NATO ASI Series, E105; Kluwer: Dordrecht, The Netherlands, 1986; p 231.
(10) Floess, J. K.; Longwell, J. P.; Sarofim, A. F. *Energy Fuels* **1988**, *2*, 18.
(11) Chu, X.; Schmidt, L. D. *Surf. Sci.* **1992**, *268*, 365.
(12) Chu, X.; Schmidt, L. D.; Chen, S. G.; Yang, R. T. *J. Catal.* **1993**, *140*, 543.
(13) Sauer, J. *Chem. Rev.* **1989**, *89*, 199.
(14) Abrahamson, J.; Maclagan, R. G. A. R. *Carbon* **1984**, *22*, 291.
(15) Chen, J. P.; Yang, R. T. *Surf. Sci.* **1989**, *216*, 481.
(16) Pan, Z. J.; Yang, R. T. *J. Catal.* **1990**, *123*, 206.
(17) Chen, S. G.; Yang, R. T.; Kapteijn, F.; Moulijn, J. A. *Ind. Eng. Chem. Res.* **1993**, *32*, 2835.
(18) Chen, S. G.; Yang, R. T. *Energy Fuels* **1997**, *11*, 421.
(19) Laurendeau, N. M. *Prog. Energy Combust. Sci.* **1978**, *4*, 221.
(20) Pan, Z.; Yang, R. T. *Ind. Eng. Chem. Res.* **1992**, *31*, 2675.
(21) Chen, N.; Yang, R. T. *Carbon*, in press.
(22) Frisch, M. J.; et al. *Gaussian 94 (Revision A.1)*; Gaussian: Pittsburgh, PA, 1995.
(23) *Handbook of Chemistry and Physics*, 67th ed.; CRC Press: Cleveland, OH, 1978; p F158.
(24) Binnig, G.; Fuchs, H.; Gerber, Ch.; Rohrer, H.; Stoll, E. T. *Europhys. Lett.* **1986**, *1*, 31.
(25) Gauthier, S.; Rousset, S.; Klein, J.; Sacks, W.; Belin, M. *J. Vac. Sci. Technol.* **1988**, *A6*, 360.
(26) Foresman, J. B.; Frisch, A. *Exploring Chemistry with Electronic Structure Methods*, 2nd ed.; Gaussian: Pittsburgh, PA, 1996.
(27) Nakamizo, M.; Honda, H.; *Carbon* **1978**, *16*, 281.
(28) Yoshizawa, K.; Okahara, K. *Carbon* **1994**, *32*, 8.
(29) Little, L. H. *Infrared Spectra of Adsorbed Species*; Academic Press: London, New York, 1971; p 326.
(30) Parikh, V. M. *Absorption Spectroscopy of Organic Molecules*; Addison-Wesley: London, 1974; p 70.
(31) Durrant, P. J.; Durrant, B. *Introduction to Advanced Inorganic Chemistry*; Wiley: New York, 1970; p 620.
(32) Cotton, F. A.; Wilkinson, G. *Advanced Inorganic Chemistry*, 2nd ed.; Interscience: New York, 1980; p 296.
(33) Moeller, T. *Inorganic Chemistry*; Wiley: New York, London, 1952; p 668.
(34) Steward, J. J. P. *QCPE Program No. 584*; Quantum Chemistry Program Exchange, Department of Chemistry, Indiana University: Bloomington, IN, 1990.
(35) Tremblay, G.; Vastola, F. J.; Walker, P. L., Jr. *Carbon* **1978**, *16*, 35.
(36) Suuberg, E. M.; Calo, J. M.; Wojtowicz, M. *Prepr/ Papers—Am. Chem. Soc., Div. Fuel* **1986**, *31* (3), 186.
(37) Kyotani, T.; Zhang, Z.; Hayashi, S.; Tomita, A. *Energy Fuels* **1988**, *6*, 136.
(38) Zhang, Z.; Kyotani, T.; Tomita, A. *Energy Fuels* **1988**, *6*, 679.
(39) Marchon, B.; Carrazza, J.; Heinemann, H.; Somorjai, G. A. *Carbon* **1988**, *26*, 506.
(40) Marchon, B.; Tysoe, W. T.; Carrazza, J.; Heinemann, H.; Somorjai, G. *J. Phys. Chem.* **1988**, *92*, 5744.
(41) Wang, J.; McEnaney, B. *Abstracts 19th American Conference on Carbon*, Pennsylvania State University, June, 25−30, 1989; American Carbon Society: University Park, PA, 1989; p. 590.
(42) Lizzio, A. A.; Jiang, H.; Radovic, L. R. *Carbon* **1990**, *28*, 7.
(43) Du, Z.; Sarofim, A. F.; Longwell, J. P. *Energy Fuels* **1990**, *4*, 296.
(44) Calo, J. M.; Hall, P. J. *Abstracts 20th American Conference on Carbon*, Santa Barbara, CA, June, 23−28, 1991; American Carbon Society: University Park, PA, 1991; p. 496.
(45) Brown, T. C.; Haynes, B. S. *Energy Fuels* **1992**, *6*, 154.
(46) Yang, R. T.; Wong, C. *J. Chem. Phys.* **1981**, *75*, 4471.
(47) Yang, R. T.; Wong, C. *Science* **1981**, *214*, 437.